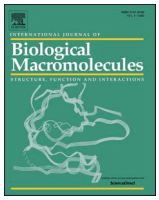
International Journal of Biological Macromolecules 310 (2025) 143084



Contents lists available at ScienceDirect

International Journal of Biological Macromolecules

journal homepage: www.elsevier.com/locate/ijbiomac



3D tubular constructs based on natural polysaccharides and recombinant polypeptide synergistic blends as potential candidates for blood vessel solutions

L.C. Rodrigues [a,b,*], J.M. Gomes [a,b], D. Soares da Costa [a,b], E.M. Fernandes [a,b], R.R. Costa [a,b], J.C. Rodriguez-Cabello [c,d], S.S. Silva [a,b], R.L. Reis [a,b]

[a] 3B's Research Group, I3Bs – Research Institute on Biomaterials, Biodegradables and Biomimetics, University of Minho, Headquarters of the European Institute of Excellence on Tissue Engineering and Regenerative Medicine, AvePark, Parque de Ciência e Tecnologia, Zona Industrial da Gandra, 4805-017 Barco, Guimarães, Portugal
[b] ICVS/3B's–PT Government Associate Laboratory, Braga/Guimarães, Portugal
[c] G.I.R. Bioforge, University of Valladolid, CIBER-BBN, Edificio LUCIA, Paseo de Belén, 19, 47011 Valladolid, Spain
[d] Networking Research Center on Bioengineering, Biomaterials, and Nanomedicine (CIBER-BBN), Valladolid, Spain

ARTICLE INFO

Keywords:
Tubular architectures
Natural polymers
Elastin recombiners
Blended formulations
Vascular endothelial growth factor (VEGF)

ABSTRACT

The development of versatile tubular structures is critical for tissue engineering (TE) applications where vascularization is necessary. This study investigates the fabrication of tubular shaped biomaterials focused on chitosan (CHT) combined with alginate (ALG) and acemannan (ACE), known for their synergistic properties, including physical stability, antibacterial activity, and healing promotion. Translating this CHT/ACE/ALG blend into 3D tubular architectures via the freeze-drying technology resulted in flexible tubes with dimensional stability, and well-defined hollow interiors. Testing these tubes for their water uptake capacity and stability indicated a substantial water absorption (about 20-fold of their dry mass), and they maintained structural integrity under physiological conditions over seven days. Structural analyses using SEM and Micro-CT revealed uniform morphology and porosity, crucial for nutrient and oxygen diffusion. Elastin-like recombinamers (ELRs) containing the QK peptide – a peptide sequence that mimics the vascular endothelial growth factor (VEGF) – were incorporated into the tubular structures, to enhance the bioactivity and the mechanical behavior of the constructs. This modification led to a reduction in porosity but without affecting endothelial cells viability, with pore size ≥100 μm was maintained. The sustained release of bioactive compounds, including ACE and ELRs, was shown to improve endothelial cells viability. Our approach thus opens new possibilities for the design of tubular structures with customizable length, diameter, stability, and bioactivity, particularly in cardiovascular applications.

1. Introduction

Tubular scaffolds are an essential component in tissue engineering, particularly for applications involving hollow organs such as blood and lymphatic vessels, urethras, and tracheas [1]. These scaffolds provide mechanical support and a structural framework for cell attachment, proliferation, and tissue regeneration. Their intricate three-dimensional morphology involves various cell types crucial for functional integrity. Current options for repairing such structures include xenografts, artificial prostheses, and autologous or synthetic grafts. Each of these options has drawbacks related to anatomical variability, tissue donor shortages, and risk of rejection [2,3]. Tissue engineering approaches employing biomaterials are therefore preferred for the replacement of diseased tissue [4–10]. The development of tubular structures has been highly explored to obtain a functional structure that can promote regeneration, repair, and replacement of damaged, injured, or lost tissue [11]. Several strategies have been employed [8,9,12–25], most of which focused on the use of tubular scaffolds composed of natural (e.g.,

* Corresponding author at: 3B's Research Group, I3Bs – Research Institute on Biomaterials, Biodegradables and Biomimetics, University of Minho, Headquarters of the European Institute of Excellence on Tissue Engineering and Regenerative Medicine, AvePark, Parque de Ciência e Tecnologia, Zona Industrial da Gandra, 4805-017 Barco, Guimarães, Portugal.
E-mail addresses: luisa.rodrigues@i3bs.uminho.pt (L.C. Rodrigues), carlos.roca@uva.es (J.C. Rodriguez-Cabello), simonesilva@i3bs.uminho.pt (S.S. Silva).

https://doi.org/10.1016/j.ijbiomac.2025.143084
Received 25 October 2024; Received in revised form 2 April 2025; Accepted 10 April 2025
Available online 17 April 2025
0141-8130/© 2025 The Authors. Published by Elsevier B.V. This is an open access article under the CC BY license (http://creativecommons.org/licenses/by/4.0/).

chitosan, collagen, hyaluronic acid, gelatin, or silk fibroin) or synthetic polymers (PCL, PLLA, PGA) [26]. Different processing strategies have been employed to obtain such tubular structures with specific characteristics: i) electrospinning produces tubular scaffolds with nanoscale fiber structures with controlled fiber alignment and diameter; ii) freeze-drying creates porous scaffolds with interconnected pore structures, able to facilitate cell infiltration and nutrient diffusion, or 3D bioprinting offers the precise deposition, spatial control of scaffold architecture and the incorporation of cells and growth factors for enhanced tissue regeneration [1,27].

Throughout their development, different obstacles have emerged, including challenges in rolling membranes around cylinder templates, achieving precise cell distribution, and ensuring adequate cell adhesion and penetration. Moreover, physical limitations such as lack of uniformity, low compliance, and inadequate biochemical and mechanical cues have hindered the creation of functional tubular structures [3,11,14,28–30]. Different strategies have been employed to address some of these drawbacks, such as using cross-linking agents by creating cell-friendly surfaces, as coatings with polyelectrolytes, or adsorption/immobilization of proteins from extracellular matrix [18,31,32]. While these constructs can be cultured under optimal conditions and show enhanced biological properties of implants, certain issues persist, including the mechanical mismatch between the host blood vessel and the artificial graft [26,33,34]. Although recent studies have produced promising results, numerous challenges remain.

One possible solution lies in the use of natural polymers. These classes of materials are often preferred over synthetic materials for fabricating scaffolds due to their biocompatibility, biodegradability, and similarity to the extracellular matrix (ECM) of native tissues [35]. Ongoing research aims to overcome existing challenges and further optimize the design and fabrication of these scaffolds for clinical translation. In this work, we hypothesize that chitosan (CHT), alginate (ALG), and acemannan (ACE) can be blended to develop versatile tubes to leverage their synergistic effects for enhanced biological and physicochemical properties. Blends of these polymers are known to generate interactions and mixed junction zones that improve biological and physicochemical features [36]. CHT, derived from chitin deacetylation, is a naturally abundant polysaccharide endowed with unique attributes, including biocompatibility, biodegradability, bactericidal activity, and processability [37–39]. When combined with ALG – another abundant natural origin polymer – it has shown enhanced wound healing efficacy [40,41]. Furthermore, the incorporation of ACE, the main polysaccharide of *aloe vera*, into the CHT/ALG mixture enhances the mechanical properties of the architectures, as in a 2D similar approach, it was possible to reinforce and modulate the stiffness and the tensile strength of the CHT/ALG system, without significantly compromising its the ductile behavior, through the variations of the ACE content [36]. As well, the release of active substances that boost biological performance, promoting fibroblast attachment, spreading, and viability, can confirm the proposed approach cytocompatibility and wound healing potential [2,36,42]. ACE is particularly notable for its ability to promote vascularization, aiding wound healing and tissue regeneration by enhancing the formation of new blood vessels [43]. This bioactive compound stimulates angiogenesis, which is crucial for delivering nutrients and oxygen to damaged tissues, thereby accelerating the healing process [42,43].

The development of tubular scaffolds made from natural polymers provides biocompatibility, bioactivity, and structural support for tissue regeneration [1,8]. Despite the promise of natural polymers, challenges remain in achieving the necessary flexibility, stability, and bioactivity to meet the functional demands of vascular applications. While existing methods allow for tuning lumen size to meet specific vascular requirements, challenges persist in simultaneously achieving precise dimensional control, material homogeneity, and biofunctional enhancement within a single scaffold. In this study, we address these challenges by fabricating flexible, versatile tubular scaffolds with precisely defined lumens using freeze-drying technology. This approach enables customizable lumen sizes and provides a unique advantage by producing scaffolds with a porous structure conducive to nutrient exchange, cell infiltration, and tissue integration, critical factors in vascular applications.

To further elevate the scaffold's functionality, the impregnation with multifunctional elastin-like recombinamers (ELRs) was hypothesized. ELRs are genetically engineered polypeptides based on the repeating pentapeptide VPG*X*G found in naturally occurring elastin, where *X* can be any natural amino acid [44–46]. The recombinant nature of these biocompatible materials allows tuning the peptide sequence to achieve advanced biofunctionalities. Herein, we employed an ELR containing the QK peptide sequence, which mimics the vascular endothelial growth factor (VEGF) [47,48]. After fabrication, physicochemical and biological assessments were conducted to validate our methodology. This innovative integration of structural specificity with advanced bioactivity represents a novel and versatile strategy for overcoming current limitations in blood vessel graft design, offering enhanced regenerative potential and paving the way for improved vascular therapies.

2. Experimental

2.1. Materials

Acemannan powder (ACE; BiAloe® Mw average 200 kPa) was supplied by Lorand Laboratories (Texas, USA). Low-viscosity sodium alginate from brown algae (ALG, ~250 cP) and chitosan (CHT) from crab shells with ca. 85 % deacetylation were supplied by Sigma-Aldrich (USA). CHT was used after purification using a reprecipitation methodology [49]. All the other used reagents and solvents were of analytical grade and used as received.

ELR recombinamers were manufactured from the previously described VKV-ELR and RGD-ELR biopolymers [50,51]. VKV-ELR includes no bioactive domains, whereas RGD-ELR contains cell-adhesive RGD sequences. Azide (N_3) and cyclooctyne groups were selected as crosslinking and grafting residues to explore a biopolymer immobilization via catalyst-free click chemistry. Firstly, VKV-ELR was modified into VKV-cyclooctyne-ELR, to be used as the counterpart for the reaction [50,52]. Secondly, N_3 groups were conjugated to the lysine (K) amino acids interspersed within RGD-ELR and VKV-ELR to produce an RGD-N_3 ELR. QK proangiogenic peptides were grafted to the RGD-N_3 ELR via dibenzocyclooctyl (DBCO) group (Bachem, Switzerland) in a 1:0.5 proportion to obtain the QK-(RGD—N_3) ELR. Characterizations of the products by proton nuclear magnetic resonance (^{1}H NMR), matrix-assisted laser desorption/ionization time-of-flight mass spectrometry (MALDI-TOF), differential scanning calorimetry (DSC), and Fourier transform infrared spectroscopy (FTIR) were published and available in the reference [53].

2.2. Solutions and tubular structures preparation

Each polymer powder was weighted and dissolved to achieve the aqueous solution of 4 % (*w/v*) concentration of each polymer (CHT, ALG, and ACE) and left to homogenize overnight, under stirring. CHT solution was prepared in hydrochloric acid (0.1 M), being its pH adjusted to 6.2–6.4, adding β-Glycerophosphate disodium salt solution (1 mg/mL). As earlier reported, ACE and ALG solutions were prepared in aqueous media [2,36,54]. Different proportions of the polymeric solutions were added and stirred, ensuring homogenization (Table 1). The

Table 1
Compositions table.

Composition	CHT	ALG	ACE
CHT/ACE/ALG (4:4:1)	44.5 %	11.0 %	44.5 %
CHT/ACE/ALG (4:3:1)	50.0 %	12.5 %	37.5 %

solutions were then casted into molds, cylindrical templates with a central pin, and freeze at −80 °C for 24 h and further freeze-dried for 72 h, according to the schematic representation in Fig. 1. ELRs solutions were prepared at 25 mg/mL ultrapure water. Subsequently, the tubular structures within the templates were impregnated, from the lumen to the border, with elastin-like recombinants, 150 μL of QK-RGD-N_3 was titrated manually into tubes ≈15 mm long. 150 μL of VKV-cyclooctine was titrated subsequently to promote the crosslink with the N_3 of the former ELR inside the tubes' porous structure. The impregnated tubes were incubated for 30 min. All steps involving ELR processing were performed at 4 °C to prevent the precipitation of the polypeptides. The impregnated tubes were frozen at −80 °C for 24 h and freeze-dried for 48-72 h. The tubular structures were detached from the templates, resulting in the formation of free-standing porous tubular structures.

2.3. Physico-chemical characterization

2.3.1. Rheology

A Malvern Instruments Kinexus rheometer equipped with a stainless steel parallel-plate sample holder of 20 mm in diameter for the oscillatory measurements and a conic plate sample holder of 40 mm for the rotational ones, and a 1 mm gap, was used to perform the rheological measurements. A fixed temperature of 25 °C was used in the rotational and oscillatory experiments. Rotational experiments allow to obtain two different plots: traditional shear viscosity (Pa.s) and shear stress (Pa) both as a function of shear rate (s^{-1}), enabling to achieve information about the flow behavior of the samples.

Oscillatory experiments were preceded by strain sweep curves to determine the linear viscoelastic region (LVER) of the samples. Strain sweeps were then performed on each different sample, acquiring 10 points per decade, from 0.01 % to 100 % at a fixed frequency of 1 Hz. Mechanical spectra were achieved, and the elastic and viscous modulus (respectively G' and G") as a function of frequency, ranging from 0.01 Hz to 100 Hz. All the tests were performed in triplicate using 1.5 mL of which solution in the sample holder.

2.3.2. FTIR

A Nicolet 6700 Spectrometer with an ATR accessorize was used to obtain Fourier transform infrared (FTIR) spectra of the samples. Each sample was prepared at room temperature, and each spectrum collected from a spectra region ranging from 4000 to 400 cm^{-1} by averaging 32 scans with a resolution of 4 cm^{-1}.

2.3.3. Scanning electron microscopy (SEM)

The morphology of the tubular structures was observed by Scanning Electron Microscopy (SEM), using Jeol JSM-6010LV microscope operated in the secondary electron mode at an accelerating voltage of 15 kV. All the samples were fixed to the aluminum stubs with double-sided carbon conductive adhesive tape and gold-sputtered using a sputter coater 108 A.

2.3.4. Micro-CT

The microstructure and architecture of the 3D tubular architectures were analyzed using microcomputed tomography (micro-CT) techniques. Samples underwent lyophilization prior to high-resolution micro-CT scanning (SkyScan 1272, Bruker, USA). Approximately 250 projections were acquired over a rotation range of 360°, with a rotation step of 0.6°. Data sets were reconstructed using the reconstruction software (NRecon 1.6.10.2 Bruker, USA), and the output format for each sample was bitmap images. Segmentation of the representative data set slices into binary images was achieved using a dynamic threshold ranging from 50 to 255. The binary images were used for morphometric analysis (CT Analyser (v1.15.4.0, Bruker, USA)) and to build the 3D models. Quantitative parameters such as total porosity (%), pore size (μm), pore distribution (%), and interconnectivity (%) were meticulously measured. Results are presented as the mean values obtained from measurements of three tubular structure samples.

2.3.5. Confocal assays

The impregnated structures were observed using a laser scanning microscope to access the distribution of CHT and ELRs into the blended structure. CHT has autofluorescence under UV light (405 nm) and ELRs were modified with Cy5 grafted in the backbone of the DBCO modified ELR allowing their observation under far red light (633 nm). The samples were imaged using the correspondent laser lines (Leica SP8) and 3D image projections were obtained using Leica LAS X 3D software.

2.3.6. Mechanical properties

The mechanical properties of the tubular structures with and without ELRs impregnation were performed under uniaxial tensile load, using an Instron 4505 universal mechanical testing equipment, at room temperature using a load cell of 50 N and a crosshead speed of 1 mm/min. The tubular structures 40 mm in length and 3.6 mm in diameter were previously gently hydrated with deionized water and placed in a pneumatic BioPlus tensile grips system at a gauge length of 15 mm. The elastic modulus, ultimate tensile strength, and strain at maximum load were obtained using the Bluehill Universal software. At least five specimens

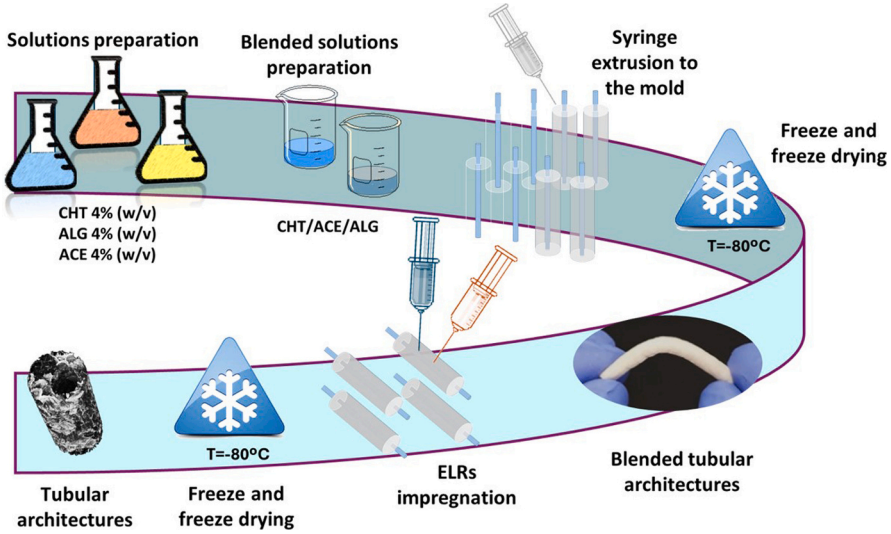


Fig. 1. Schematic representation of the methodology of preparation of the tubular architectures and compositions table (Table 1).

per condition were tested, and the results are expressed in mean ± standard deviation.

2.3.7. Swelling and release assays

2.3.7.1. Water uptake quantification. Structures of 1 cm length were soaked into PBS buffer solution, at 37 °C to access the water uptake and ACE release profile of the films. The swollen samples were extracted from the buffer solution at predefined time points (15 min, 30 min, 45 min, 1 h, 2 h, 3 h, 4 h, 5 h, 6 h, 24 h, 2d, 4d and 5d) and the excess of solution removed with filter paper (Filter Lab, Spain). Thus, the samples weight were accessed using an analytical balance (Denver Instrument, Germany). All the assays were performed in triplicate ($n = 3$). The water uptake was calculated as follows:

$$\text{Water uptake } (\%) = \frac{W_w - W_d}{W_d} \times 100$$

where W_w and W_d are the weights of swollen and dried films, respectively.

2.3.7.2. ACE release quantification. Similarly to the water uptake procedure earlier described, the structures were soaked at 37 °C into PBS incubation media, along 10 days, under mild agitation to improve the diffusion through the incubating media. At predefined time points, the surrounding buffer media were removed from each container, and the experiments performed in triplicate ($n = 3$). Considering a homogeneous distribution into the structure, the total mass of ACE in the structure was considered to be 100 % ACE.

A calibration curve was constructed based on ten ACE concentrations, between 2.5×10^{-4} g.mL^{-1} and 5.0×10^{-2} g.mL^{-1}, in PBS buffer media, from which absorbance was measured at 300 nm. The absorbance of the retrieved samples was measured at the same wavelength, and the values achieved were comparatively studied within a previously constructed calibration curve.

2.3.7.3. ELRs release quantification. Similarly, to the ACE release procedure earlier described, the structures were soaked at 37 °C into PBS incubation media, along 10 days, under mild agitation to improve the diffusion through the incubating media. At predefined time points, the surrounding buffer media were removed from each container, and the experiments were performed in triplicate ($n = 3$). Considering a homogeneous distribution in the structure, the total mass of impregnated ELRs (7.5 μg/tubular structure) in the structure was considered to be 100 % ELRs.

A calibration curve was constructed based on six ELRs concentrations, between 7.8×10^{-3} mg.mL^{-1} and 1.0 g.mL^{-1}, in PBS buffer media, from which fluorescence was measured at Ex/Em 646/662 nm. The fluorescence of the retrieved samples was measured at the same wavelength and the achieved values were comparatively studied within a previously constructed calibration curve.

2.3.8. Cell viability assays

Before cell culture studies, the structures were sterilized using ethylene oxide. Direct contact tests employing the immortalized human vascular endothelial Cells (EA.hy926) were conducted. Cells were cultured in basic medium: Dulbecco's modified Eagle's medium (DMEM; Sigma-Aldrich, USA) with phenol red, with 10 % fetal bovine serum (Life Technologies, USA) and 1 % antibiotic/antimycotic (A/A, Gibco, UK) solution. EA.hy926 cells were incubated at 37 °C in an atmosphere containing 5 % of CO_2 until 90 % confluence was achieved. The tubular structures were placed into non-adherent 24-well plates, and cells were seeded onto them dropwise at a cellular density of 2×10^4 cells/structure. The samples were analyzed after 1, 3, and 7 days of culturing in DMEM at 37 °C in a humidified atmosphere with 5 % CO_2. Tissue culture polystyrene (TCP) served as a control and was maintained under identical conditions for the same duration. The culture medium was replaced twice a week throughout the experiment.

The metabolic activity of cells seeded on the tubular structures was evaluated using the CellTiter 96 AQueous One Solution Cell Proliferation Assay (MTS, Promega). Briefly, cell−scaffold constructs were placed in a mixture containing serum-free cell culture medium and MTS reagent at a 5:1 ratio and incubated for 3 h, at the end of which the optical density was read (OD 490 nm).

The cell viability was also evaluated by fluorescence labeling using a live/dead assay. For this purpose, the designed tubular architectures were removed from the culture medium and washed with sterile PBS. Subsequently, all samples were incubated with 1 mg/mL calcein acetoxymethyl (Invitrogen, 1:500) and 1.5 mM propidium iodide Invitrogen, 1:1000) solution in PBS for 15 min, at 37 °C and washed with sterile PBS. After this, the samples were imaged using a confocal laser scanning microscope (Leica SP8). *Z*-stacks of all samples were acquired, and maximum projections were obtained, showing viable cells green (Calcein AM) and nonviable cells red (PI). The laser settings were 488 and 561 nm for Calcein AM and PI, respectively. The software LAX was used to analyze the images. Quantification of the viable cells was performed using ImageJ (analysis of particles macro), and data was represented as the percentage of viable cells.

2.3.9. Statistical data treatment

All the experimental tests were conducted in triplicate ($n = 3$), and the achieved data points are presented as the mean ± standard deviation. Statistical analysis was performed while using the GraphPad Prism 5.0 software. The data that demonstrated a normal distribution were analyzed using a one-way ANOVA (for the remaining, a non-parametric Kruskal-Wallis test was used). In addition, the statistical analysis for the mechanical tests ($n = 6$) was performed using the Krustal-Wallis test with Dunn's comparison to determine statistical differences. The significance level between the groups was set for * $p < 0.05$, ** $p < 0.01$, *** $p < 0.001$, and **** $p < 0.0001$. The data were presented as mean ± standard deviation (SD).

3. Results and discussion

3.1. Solutions properties assessment

3D structures design through freeze-drying methods requires careful analyses of the physical properties of the employed solutions. These solutions must meet specific rheological requirements, with the right balance of viscosity, yield stress, and thixotropy, exhibit temperature-dependent gelation, be homogeneous, and have controlled freezing characteristics to ensure successful shaping, stability during freezing, and proper sublimation during drying [55]. The solutions should ensure a consistent balance that allows them to be extruded into the mold without leaking out.

The shear viscosity plotted against the shear rate for the prepared solutions is depicted in Fig. 2-A. At low shear rates (<~10 s^{-1}), the viscosities of CHT/ACE/ALG solutions surpass those of individual polymer solutions, even though remaining lower than those reported for similar CHT/ACE/ALG formulations with smaller initial polymer solution concentrations [36]. These findings suggest that increasing the initial polymer solution concentration influenced polymer chain interactions, enabling a near-complete mitigation of ACE's non-gelling ability. The increase in the number of polymeric chains per unit of volume leads to a more efficient balance of hydrophilic and hydrophobic interactions between the polymers and, may also favor the physical interaction due to an increase of calcium ion presence (in traces as a residue of the ACE extraction from AV leaves) in the solution that potentiates ALG gelation or even, through the CHT and ALG well-known electrostatic interactions.

The fitting of the experimental data presented in Fig. 2-B was performed according to the power-law model: $y = kx^n$, where y is the shear

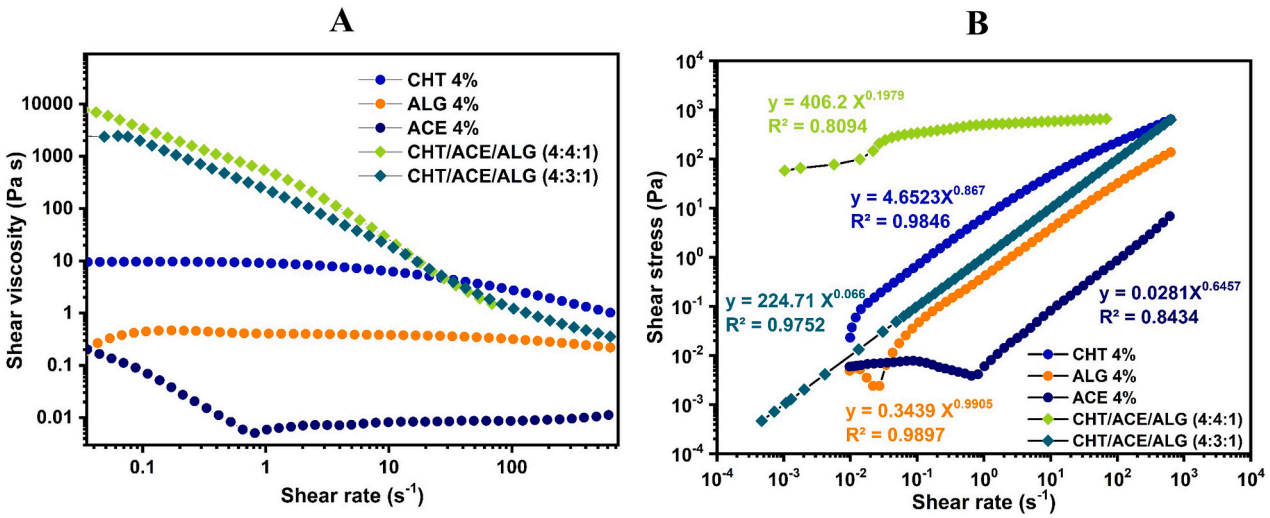


Fig. 2. Viscosimetry assays of CHT/ACE/ALG blended solutions. (A) Viscosity curves of the individual polymeric and blended ternary solutions as a function of shear rate; and (B) Shear stress curves as a function of the shear rate with adjusted power-law equations.

stress (Pa), x is the shear rate (s^{-1}), k is the consistency coefficient (Pa. s^n), and n is the flow behavior index, allowing to define the flow behavior of each solution [56,57]. The adjusted power laws, allowed us to note that only the ALG polymeric solution ($n = 0.99 \pm 0.04$) presents a Newtonian fluid flow behavior (n near 1), and all the remaining solutions (blended formulation and CHT and ACE solutions) present an n lower than 1, which is consistent with a pseudoplastic fluid (shear-thinning) flow behavior [57].

An appropriate viscosity allows the extrusion and avoids structure collapse, being the shear-thinning (pseudoplastic) behavior often preferred [55]. The material should hold its shape under its weight and after any stress is applied during processing, this may be modulated through the adjustment of the solution yield stress, by modifying the concentration and ratio of the polymers in the solution. The control of these properties ensures that the solutions can be processed into the desired shape, maintaining their integrity during freezing and resulting in a stable, porous structure [55]. Their evaluation will allow the adjustment of the solution formulation through the use of different polymeric ratios, demonstrating the adaptability and potential versatility of the solutions.

The storage modulus (G') and the loss modulus (G") as a function of frequency, at 25 °C, were registered in Fig. 3A. G' and G" curves tend to a plateau most likely independent of the frequency, especially for lower values of frequencies (0.1–1 Hz). Reaching higher frequencies, is noted an increase of the registered G' and G", which is similar to the studied blended formulations. The establishment of a network structure between the polymeric chains, promoted an increase of the formulations resistance to deformation [58], justifying the significant increase of G' and G" observed from the isolated polymer solution and the blended formulations. For instance, we can observe that the oscillatory curves for the ACE and ALG solutions exhibited extremely low G' and G" values (both below 2 Pa, see Fig. 3A), indicating a highly fluid state. However, when the polymers were combined in the CHT/ACE/ALG 4:4:1 formulation, the G' value increased dramatically to 4058.32 ± 32.15 Pa with a corresponding G" value of 665.63 ± 6.67 Pa, values at a frequency of 1 Hz. Similar high G' and G" values were also observed for CHT/ACE/ALG 4:3:1 at the same frequency (1 Hz). This significant increase in both moduli demonstrates the formation of a strong and elastic network within the formulations, driven by interactions, mainly due to ALG gelation promoted by the Ca^{2+} of the ACE solution, the well-documented electrostatic interaction of CHT and ALG, and the hydrophilic and hydrophobic interactions between the chains, as previously

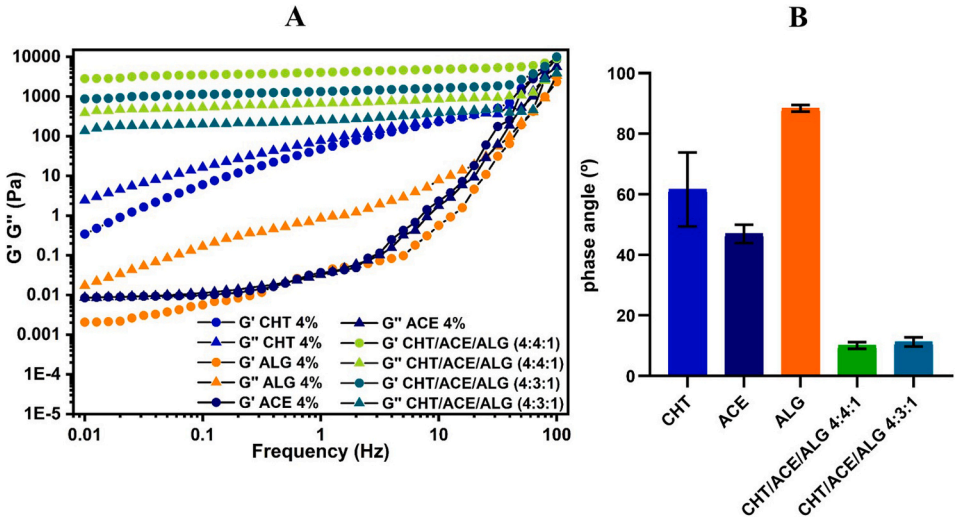


Fig. 3. Oscillatory assays of CHT/ACE/ALG blended solutions. (A) Oscillatory curves of the individual polymers and blended ternary solutions as a function of frequency; and (B) Phase angle values.

hypothesized in other studies [36,59]. Our formulation successfully addressed the non-gelling characteristic of ACE. Unlike previous studies where formulations with higher ACE content exhibited reduced strength, this issue was not observed in the current study. Similarly to the reported blended formulations prepared using 2 % solutions [36], all blended formulations have higher storage than loss moduli values, confirming the prevalence of a gel character consequence of the enhanced stability of the formed network. The higher elastic behavior registered is observed for the CHT/ACE/ALG 4:4:1 formulation, suggesting that this composition, in solution, presents a stronger interaction between the polymeric chains. This is in accordance with the phase angle values achieved for the blended formulations, which are lower than 20°, suggesting a gel-like state, where the material at rest is solid, such as pastes, gels, or other stiff solid matter, confirming the strong interactions established between the polymeric networks [60,61].

3.2. Tubular architectures chemical interactions – FTIR

CHT, ALG, and ACE structural differences that occurred in the blended architectures were studied by FTIR analysis before and after ELR's impregnation. The polymers' main characteristic peaks of each region can be observed on the spectrum presented in Fig. 4, as the saccharide peaks (900–1200 cm^{-1}) that are representative of the skeletal vibrations associated with C–O–C glycosidic bonds [62–65]. Moreover, the bands associated with the amide II band (NH_2 stretching) (1535 cm^{-1}), and amide I (-NH-C=O stretching) (1630–1700 cm^{-1}) [64,65], appear proportionally to CHT's ratio in the blends.

The characteristic transmittance bands of C═O stretching, present at 1730 cm^{-1}, indicating carbonyl groups on ACE are also noticeable in the spectrum of the blended architectures [66].

Furthermore, the carboxyl asymmetric group and the hydroxyl group band at 3410–3425 cm^{-1} (not included in the figure range) as some other ALG bands undergo a slight increase on the wavenumber. This observation is in accordance with other ALG's combinations already reported [36,67], suggesting good molecular affinity and the formation of chemical interactions between the polymers.

Considering the impregnated tubular architectures (samples C and D) the amides I and II related to the ELR's are significantly more pronounced than on the uncoated samples (A and B), confirming the presence of the ELR's coating in the tubular structure. Similar behavior was earlier reported for the coating and impregnation of ELRs into expanded polytetrafluoroethylene (ePTFE) vascular grafts [68].

3.3. Tubular architectures morphological studies

The tubular structures were built up using 4 % CHT, ACE, and ALG solution to prepare blended formulations in different polymeric ratios. The fabrication procedure involved casting the blended formulations onto cylindrical templates with a central pin, followed by two freeze-drying cycles, one before ELRs impregnation and another after. The structures were then easily detached from the templates, obtaining free-standing porous tubular structures. CHT/ACE/ALG stable tubular

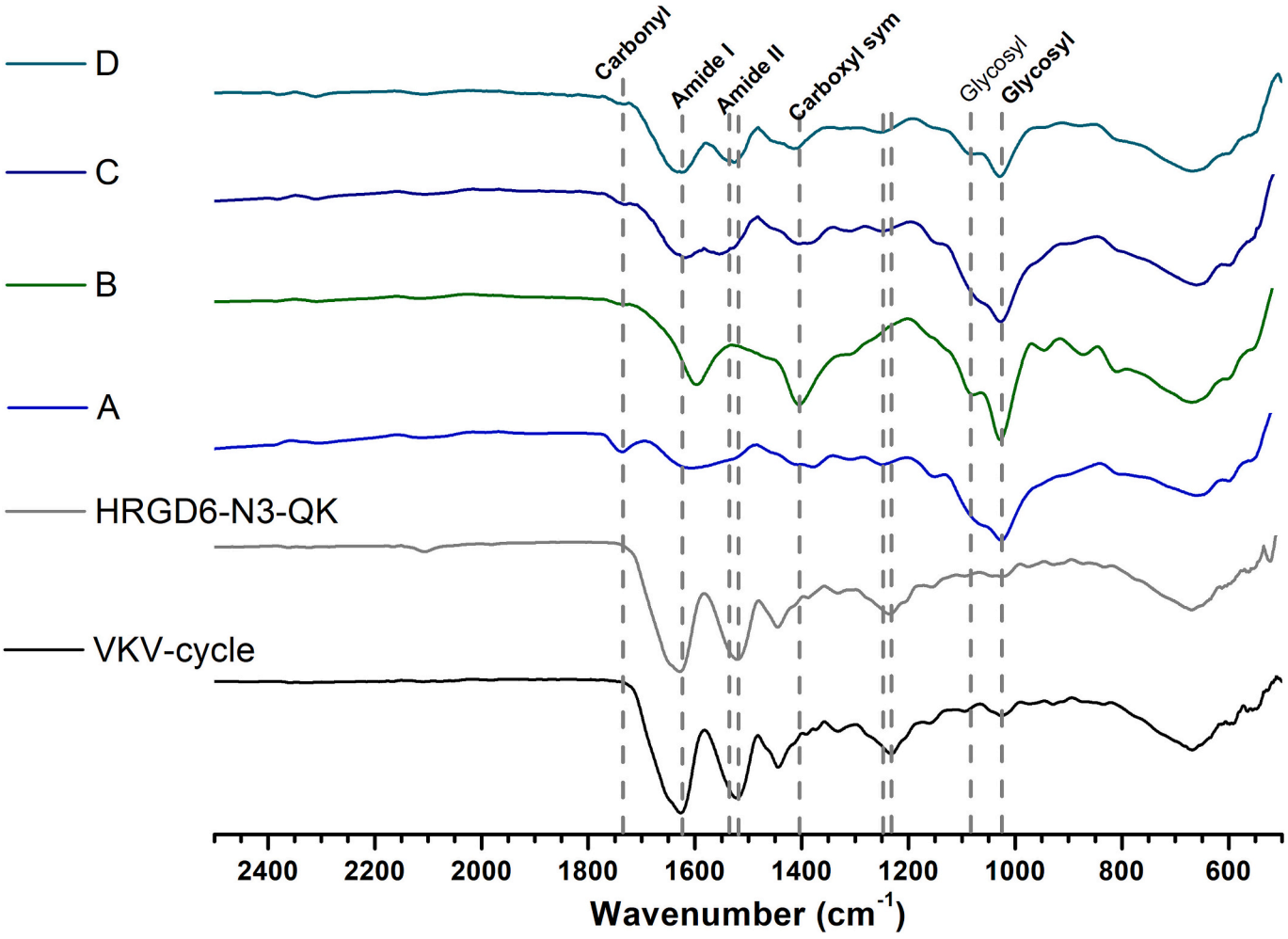


Fig. 4. FTIR spectra of the used ELR's and the produced tubular architectures without ELR's impregnation (A and B) and with ELR's impregnation (C and D). (A and C compositon 4:3:1) and (B and D composition 4:4:1).

structures, with different polymeric proportions, were achieved with a defined diameter (dependent on the diameter of the used template). Macroscopically, these tubes exhibited smooth surfaces and minimal defects.

SEM (Fig. 5 A and B) was used to evaluate the morphology of the developed CHT/ACE/ALG tubular structures, demonstrating a uniform tubular structure free of defects (i.e., cracks and holes) and highlighting the efficiency of the approach. This tubular structure allowed for the impregnation with proangiogenic ELRs, namely QK-RGD. The utilized QK peptide is a VEGF-mimicking peptide consisting of a string of KLTWQELYQLKYKGI amino acids, which – taking advantage of the genetically engineered nature of ELRs – was embedded alongside the VPG*X*G elastin pentapetide. The impregnation of QK-RGD in these tubes applies the click-chemistry principle used in the hydrogel-forming structures described by Flora et al. [48,69,70]. Concretely, we first impregnated the inner part of the tubes with the VKV-cyclooctine to support the chemically covalent binding of QK-RGD-N_3. The aim was to act as a structure coating on the lumen and the walls of the pores.

The choice of ELR coating via impregnation was made to ensure a uniform distribution of bioactive chemical cues across the entire scaffold, addressing the inherent structural and functional differences between the inner and outer layers of the tubular scaffold. The coating process was conducted via impregnation, proceeding from the lumen to the outer border of the scaffold, to establish a gradient in the distribution of bioactive chemical cues across its structure [71]. This gradient was designed to achieve a higher concentration of bioactive agents at the lumen, targeting interactions with endothelial cells while gradually decreasing towards the scaffold's border, which is tailored to support smooth muscle cells or fibroblasts. This strategic approach enables the scaffold to address the intrinsic structural and functional differences between its inner and outer layers, effectively mimicking the natural heterogeneity of blood vessels. By replicating these biological gradients, the proposed method holds significant potential for enhancing the scaffold's biocompatibility and functional integration in vascular tissue engineering.

In fact, comparing all the structures from different formulations, we showed that the ELR's impregnation did not significantly decrease the pore size throughout the wall and interior of the tubes, representing only

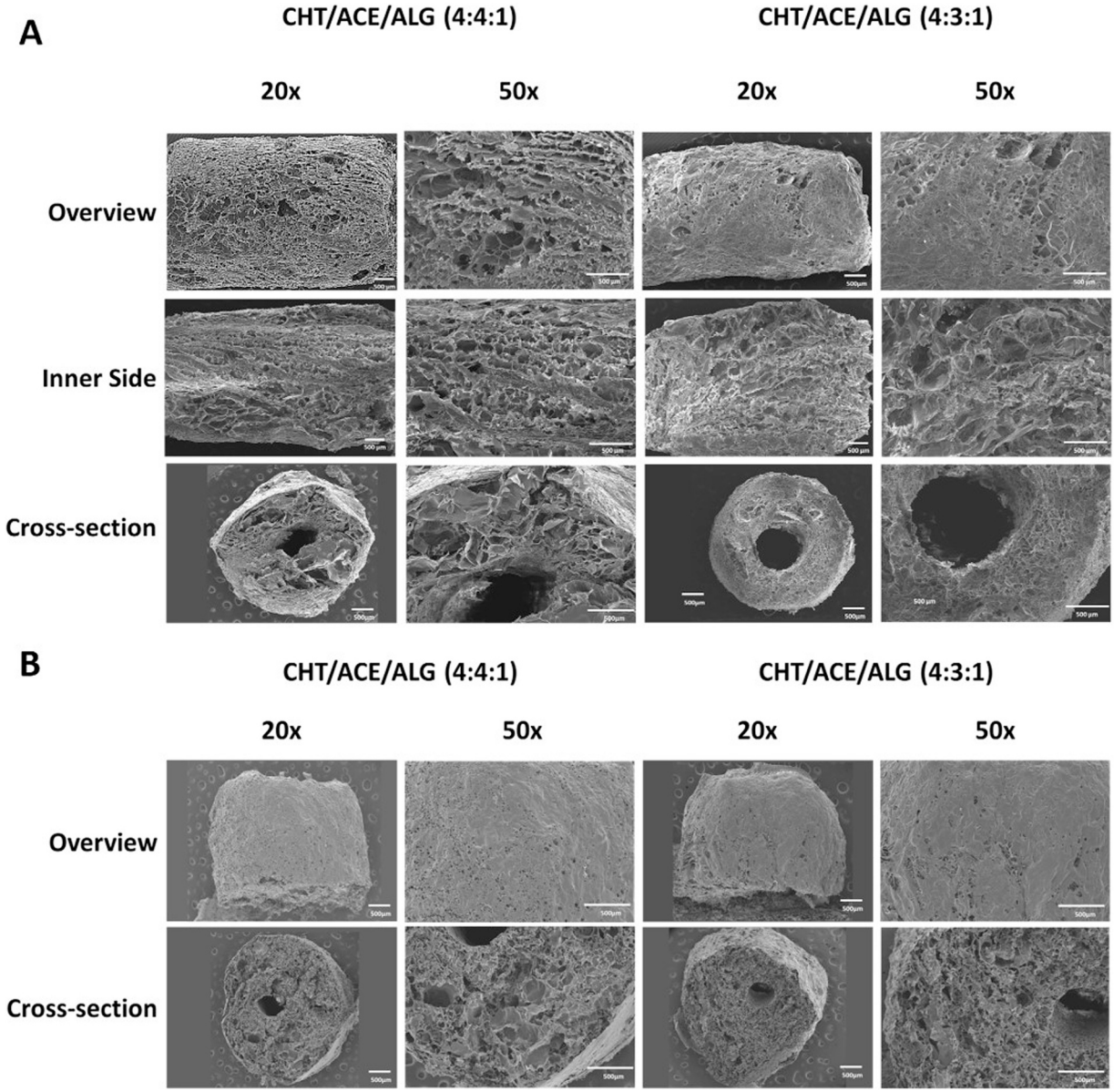


Fig. 5. (A) Tube morphology: SEM images of CHT/ACE/ALG blended tubes (scale bar 500 μm) and (B) CHT/ACE/ALG blended tubes impregnated with ELRs (scale bar 500 μm).

0.4 % of the total mass of the structure. This observation is aligned with earlier reports where ELRs coatings do not affect the microstructure and porosity of the device [68].

Similar results were achieved by micro-CT analysis (Fig. 6 and Table 2): no significant differences were observed between the tubular formulations, and thus only a representative micro-CT image is shown. The average pore size of each formulation remains similar after ELRs impregnation however, a significant reduction of porosity was observed (from around 60 % to 20 %). This behavior is attributed to the impregnation of ELR solution into the structure, which, after cross-linking, may form aggregates able to block some of the existing pores. This confirms the retention of ELRs within the pores of the produced 3D architectures, creating a porous thin layer of elastin-mimetic polypeptide [68,70]. This fact is aligned with the pore size distribution data, where an increase of the incidence of smaller pores (19-57 μm, respectively, from 6.7 % to 35.1 %) is noted for the impregnated samples. The remaining pore sizes maintain a similar distribution profile after impregnation, with 60 % of the pores still ranging between 57 and 320 μm. According to this, all the studied tubular structures (from both formulations) exhibit pore sizes higher than the minimum required for cell attachment and proliferation, facilitating tissue growth and diffusion of nutrients and oxygen (100 μm in diameter) [8,72,73]. This confirms their potential to be applied in tissue engineering approaches.

The confocal images of the impregnated structures (Fig. 7) allowed us to analyze the distribution of CHT polymeric chains into the blended structure, including ELR's distribution after impregnation.

With CHT being the main constituent of the blended formulation, it was expected to be distributed throughout the structure, thereby defining its shape. The auto-fluorescence of CHT (in blue) allowed observation of its distribution within the tubular structure, revealing well-defined pores similar to those observed in the micro-CT scans. This supports the hypothesis that CHT serves as the backbone of the designed architecture. The ELRs impregnated in the structure (in red) were almost homogeneously distributed, covering the walls of both the outer surface and the pores, leading to a reduction in porosity. This observation aligns with the micro-CT results, which also indicated a decrease in the tubular structures' porosity due to the ELR coating (Table 2).

The tubular structures developed exhibited key properties relevant to tissue engineering applications, as illustrated in Fig. 8. The images demonstrate the versatility of the fabrication process, allowing for the production of tubes with varying diameters by utilizing different external molds (Fig. 8A). This adaptability in dimension highlights the potential for customization to meet specific anatomical and functional requirements. Additionally, the structures displayed notable flexibility and bending capability (Fig. 8B), suggesting their potential for dynamic environments where mechanical compliance is crucial. Furthermore, the suitability of the tubes for suturing, as depicted in Fig. 8C, indicates their potential for practical surgical applications, where secure attachment and integration with biological tissues are essential.

Table 2
Mean pore size, porosity, and pores interconnectivity data achieved by Micro-CT analysis.

	CHT/ACE/ALG formulation	Mean pore size (μm)	Porosity (%)
Without ELR's	4:4:1	110 ± 30	66.74 ± 6.41
	4:3:1	120 ± 10	60.41 ± 3.35
With ELR's	4:4:1	140 ± 10	27.20 ± 1.65
	4:3:1	140 ± 10	24.10 ± 1.03

3.4. Mechanical properties

Given the importance of mechanical properties in tissue engineering, mechanical assays were conducted to further evaluate the structural integrity and performance of the developed tubular constructs. The dimensional stability of the ternary systems composed of CHT/ACE/ALG at varying ratios, both before and after impregnation with ELRs, were evaluated under uniaxial tensile load in hydrated state, and the main properties are reported in Fig. 9. The developed polymeric tubular structures targeting tissue engineering applications showed properties in the range of Kpa, revealing significant statistical differences in composition and when impregnated with ELRs. In more detail, the lower elastic modulus values of 29.9 ± 5.8 KPa up to 33.9 ± 5.0 KPa were obtained for both compositions without ELRs (Fig. 9 A). After ELRs impregnation it was observed an increase in the mechanical properties in terms of stiffness and ultimate tensile strength reaching higher values up to 152.4 ± 41.4 KPa for the elastic modulus and 15.86 ± 2.0 KPa for the ultimate tensile strength, respectively (Fig. 9 A - B). A similar trend in the mechanical behavior was observed in collagen-based tubular gels combined with elastins [74]. Moreover and regarding the reduction of the ACE content, revealed a significant increase in the ultimate tensile strength and in the strain at maximum load without significantly compromising the stiffness of the tubular structure. This might occur due to the higher interaction between CHT and ALG components in the system, which is in agreement with the observed rheology results of the constituents under shear stress. It was also noticed that all the compositions show a ductile behavior (Fig. 9 C) with strain values at maximum load ranging from 13.4 ± 3.6 % for CHT/ACE/ALG (4:4:1) + ELRs and 44.2 ± 6.9 % for CHT/ACE/ALG (4:3:1) respectively. The deformation capability of the polymeric tubular structures presents higher strain values at break; however, it is important to notice that after reaching the ultimate tensile strength values the stress-strain curve reduces progressively, compromising the integrity of the tubular structure.

3.5. Swelling ability and release profile

The swelling ability of the prepared blended tubular structures without and with ELR's impregnation was studied for 5 days at 37 °C. A similar profile was observed between compositions; however, a

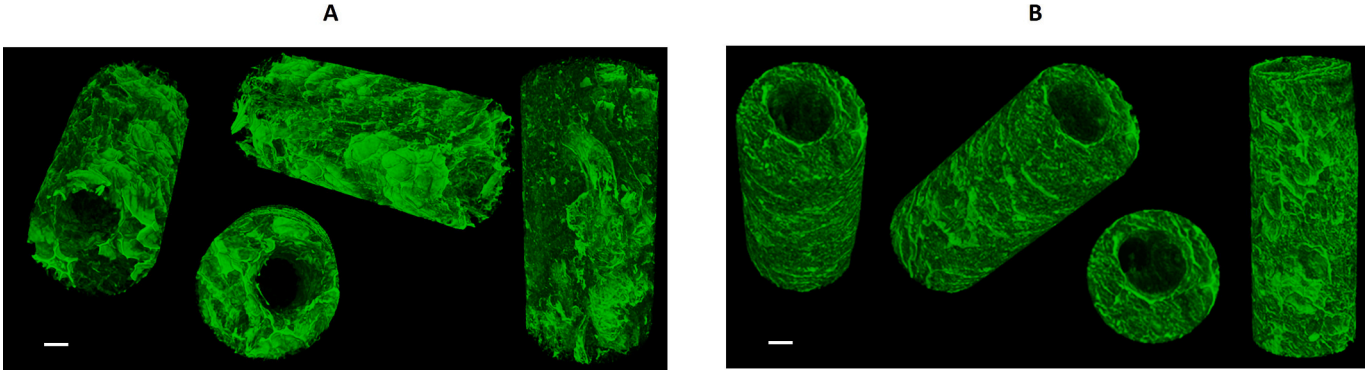


Fig. 6. Tube morphology: Micro-CT micrographs of CHT/ACE/ALG (4:4:1) blended tubes: (A) non-impregnated and (B) impregnated with ELRs. (scale bar 100 μm).

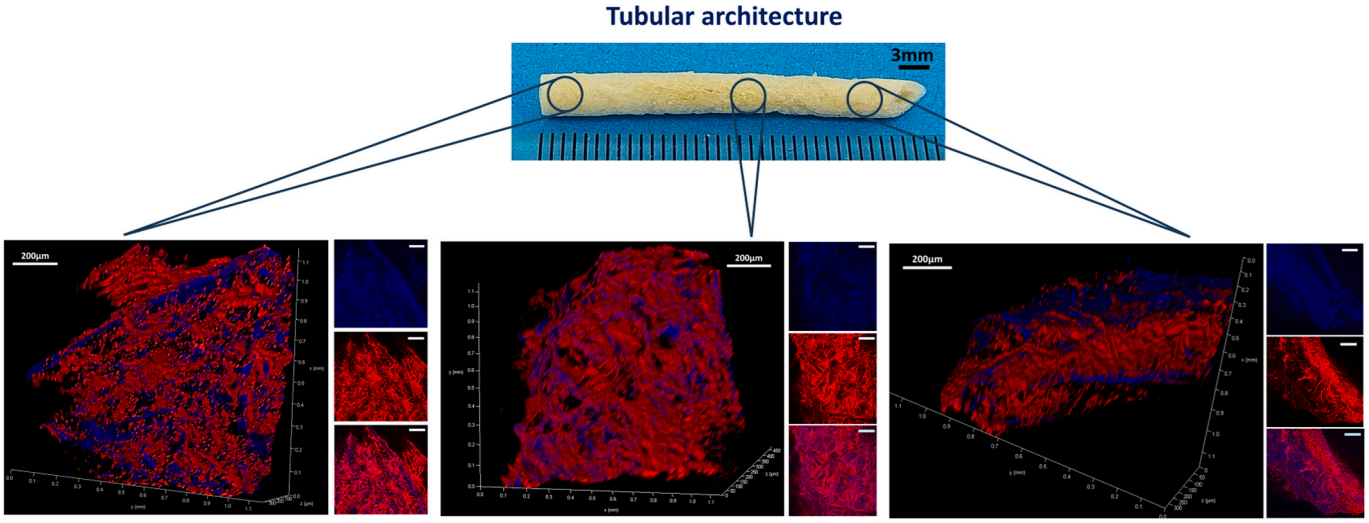


Fig. 7. Tube morphology: Different regions confocal micrographs of CHT/ACE/ALG (4:4:1) blended tubes impregnated with ELRs being the elastin fluorescence in red and CHT auto-fluorescence in blue. Scale bars correspond to 200 µm. (For interpretation of the references to colour in this figure legend, the reader is referred to the web version of this article.)

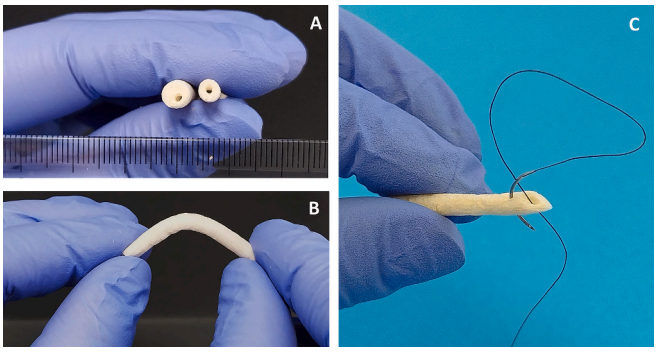


Fig. 8. Representative images of tubular structures illustrating: (A) variation in diameters achieved using different external molds; (B) flexibility and bending ability; and (C) suitability for suturing (size 5).

significant difference was observed between the impregnated and non-impregnated structures (Fig. 10A). Considering the non-impregnated samples group, there is a similarity between compositions that is in accordance with the earlier reported results related to blended films with similar polymeric composition and CHT-based tubular architectures without cross-linking [8,36]. The impregnation of the structures with the recombinant ELRs significantly reduced the water uptake ability. This fact may be related to the observed reduction of porosity that makes it difficult for water permeation into the structure as also to the strength of the crosslinking at the surface of the polymeric architecture, which reduces water affinity due to the hydrophobic nature of the ELRs [75,76]. This result favors the potential of the designed system, as it suggests a structural stability of the structures in wet environments, to have a reduced variability of its volumetry.

The correlation of the mass loss and the ACE release results suggest that the ELRs impregnated at the tubular polymeric structures are released after immersion in PBS for 7 days, as the mass loss percentage for the impregnated structures is significantly higher (45 and 52 %) than for the non-impregnated ones (13 and 18 %), being significative the differences on mass observed between samples of the same composition with and without ELRs impregnation. Comparing the results, it is likely that the release of ELR may weaken the polymeric network, despite representing only 0.4 % of the structure, the mass loss increases by around 30 %, suggesting a microfragmentation of the polymeric

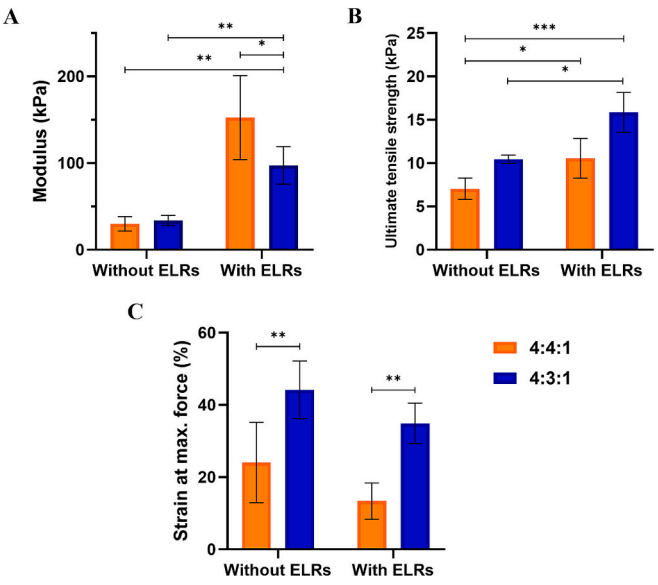


Fig. 9. Tensile properties of the CHT/ACE/ALG tubular structures, with and without ELRs impregnation, (A) elastic modulus; (B) ultimate tensile strength; and (C) strain at maximum force. Significant differences were assigned with ****, ***, ** and * respectively for $p < 0.0001$, $p < 0.001$, $p < 0.01$ and $p < 0.05$.

structure in the media.

Considering the amount of ACE released to the media (Fig. 10C), the achieved profile is similar between all the compositions, with only a slightly higher release from the non-impregnated samples. Similarly to earlier reports for blended formulations using the same ratio and polymers, the formulations 4:3:1 are the ones with smaller ACE release in PBS for each group [36]. This is attributed to the strongest chemical interactions between the polymeric chains on this polymeric ratio, which enhance the entrapment of ACE molecules within the structure. This result agrees with the earlier reported study of the solvent casting blended films mechanical evaluation assays, which reveal that the 4:3:1 composition exhibits superior network stability [36]. When comparing samples of the same composition with and without ELRs impregnation, the impregnated samples exhibit lower ACE release. This may be related

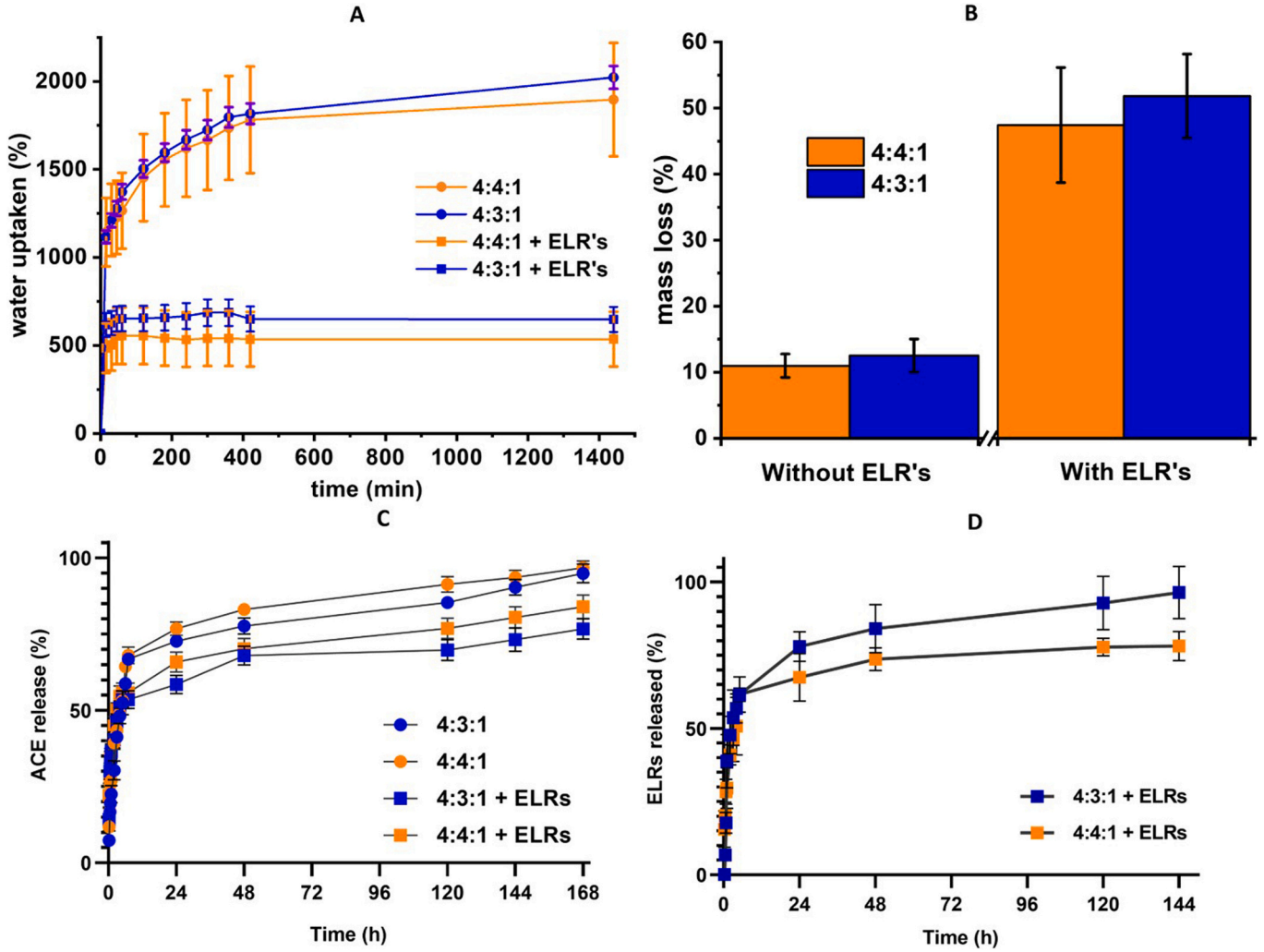


Fig. 10. (A) Water uptake ability of the produced tubular architectures without and with ELR's impregnation; (B) Mass lost after 7 days in PBS of the produced tubular architectures without and with ELR's impregnation; (C) ACE release quantification from the produced tubular architectures without and with ELR's impregnation; and (D) ELRs release quantification from the produced tubular architectures with ELR's impregnation.

to the observed reductions in water uptake in these samples. According to this, it was hypothesized that a lower water penetration on the structure does not favor the water-soluble ACE release from the structure and consequent migration to the surrounding media. The quantification of ELR release (Fig. 10D) indicates a substantial release (i.e., above 70 %) of the impregnated ELRs into the surrounding media for both tubular formulations. Overall, no significant differences were observed between the release profiles of the two formulations, which exhibited similar behavior characterized by an initial burst release during the first few hours, followed by a plateau after 24 h. The slightly higher ELR release observed for the 4:3:1 formulation at longer time points aligns well with the trend observed in the mass loss assays, which may suggest that structures with higher ACE ratios also support better ELR's physical impregnation.

3.6. Direct contact with endothelial cell line

To evaluate the potential of the designed architectures for tissue engineering applications, the cytotoxicity of the developed tubes was assessed. Given that no significant differences were observed between the ternary compositions, both demonstrating comparable performance in the physicochemical tests, the in-vitro assays were conducted using the 4:4:1 formulation. This formulation was selected due to its higher ACE content, which is expected to have a positive influence on cell performance. Additionally, to investigate the specific effect of ACE incorporation within the formulation, experiments were performed using structures consisting solely of CHT and ALG (CHT/ALG), while maintaining the same polymeric ratio as in the ternary system. We have observed an increase in cell metabolic activity over time (Fig. 11A), significantly more evident for the sample containing ACE and ELRs. Comparing CHT/ALG with CHT/ALG/ACE formulation, those containing ACE showed increased metabolic activity, especially on days 1 and 3. A similar effect was observed for the CHT/ALG + ELR samples, where the ELR release to the media enhanced cell metabolic activity over time. According to the literature, it is known that ACE is not toxic to fibroblasts and endothelial cells, and it has significantly stimulated the proliferation of gingival fibroblasts and the expression of vascular endothelial growth factor (VEGF) [36,43,77]. ACE can bind to mannose residues present in fibroblast surface receptors, triggering the secretion of important growth factors and extracellular matrix proteins that stimulate cell proliferation [36,43], increasing cell viability in damaged or healthy cells, owing to its antioxidant effect. Besides the less pronounced ACE effect in endothelial cells, an in vitro study demonstrated an up-regulatory effect on TGF-β1 and VEGF gene expression in a dose-dependent and time-dependent manner [78]. These studies corroborate the positive effect we observed with the formulations containing ACE [36,43,78]. Moreover, these results are aligned with a previous investigation, which demonstrated that scaffolds coated with tropoelastin

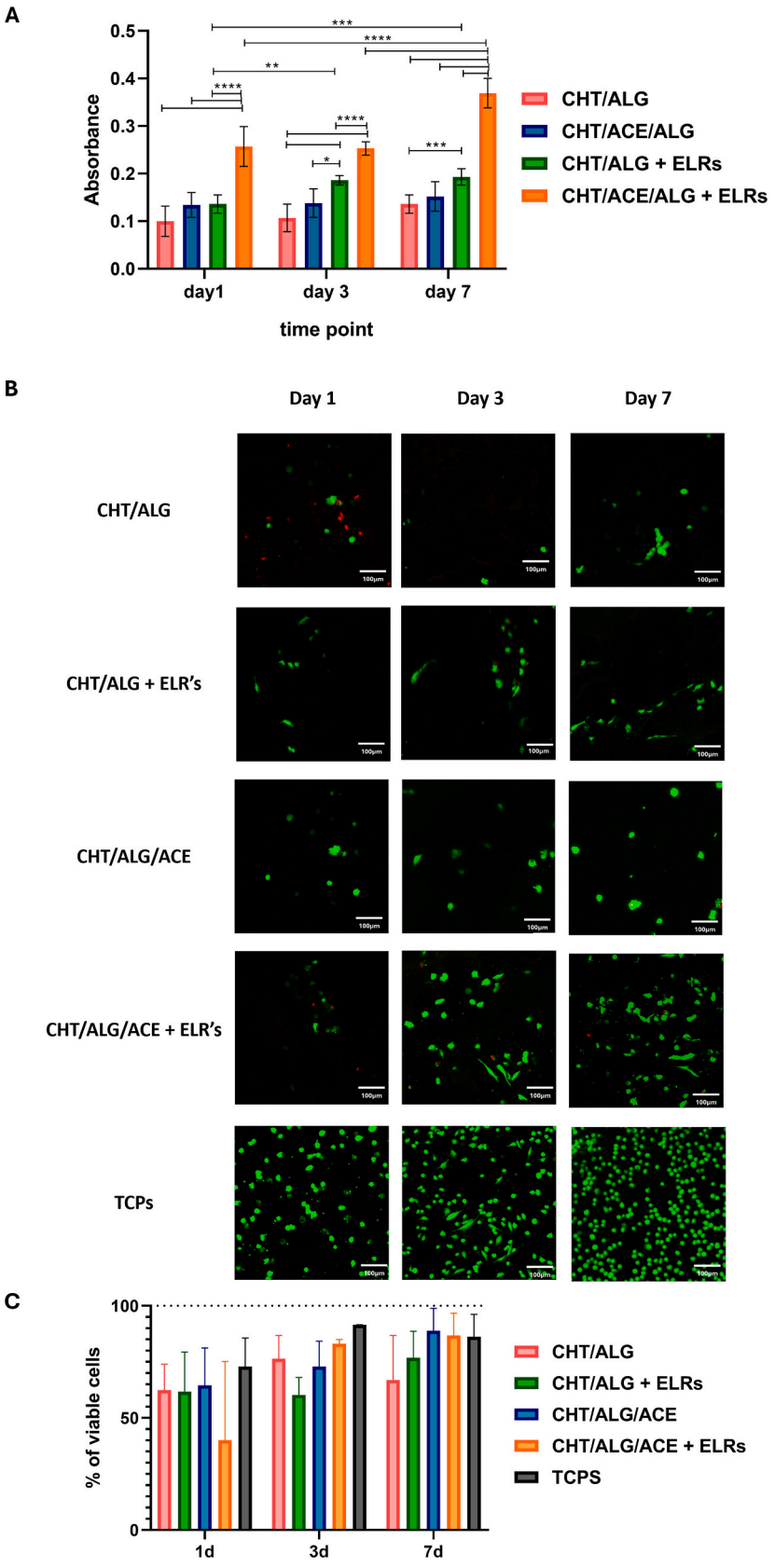


Fig. 11. (A) Metabolic activity after 1, 3, and 7 days of culture. Significant differences were assigned with ****, ***, ** and * respectively for $p < 0.0001$, $p < 0.001$, $p < 0.01$ and $p < 0.05$; (B) Cell viability assay (live-dead staining) after 1,3 and 7 days, scale bar 100 μm; and (C) Quantification of cell viability represented as % of viable cells.

inhibit the development of intimal hyperplasia, thereby promoting the attachment and proliferation of endothelial cells [79]. In a separate study [80], it was observed that exposed elastin sequences can elevate the levels of matrix metalloproteinases (MMP-2), which facilitate the degradation of connective tissue growth factor (CTGF). This degradation, in conjunction with transforming growth factor-beta 1 (TGF-β1), increases the concentration of free vascular endothelial growth factor (VEGF), thereby enhancing angiogenic activity [80].

Blending different polymers can help to tailor the system properties and behavior [35]. We observed a synergistic effect in the formulation containing both ACE and ELRs. Cell contact assays showed that samples with ACE and ELRs exhibited higher metabolic activity and a significant improvement in cell adhesion and viability (Fig. 11B and C). Cells often do not adhere well to CHT/ALG structures because both polymers are highly hydrophilic and lack sufficient adhesion points. In contrast, ACE, a bioactive polysaccharide, provides ECM-like properties due to the presence of functional groups that mimic ECM structures, thus encouraging cell adhesion [81]. Moreover, ACE also supports signaling pathways associated with wound healing and tissue regeneration. The incorporation of ELRs in the system provides additional cell-adhesive domains, due to the presence of RGD sequences, which integrin receptors on cell membranes readily recognize.

The combination of ACE and ELRs with CHT/ALG enhances surface characteristics, offering a better balance between hydrophilicity and bioactivity. The improved microenvironment supports cell attachment and proliferation more effectively than the CHT/ALG alone. Collectively, ACE and ELRs provide chemical and structural cues that bridge the gap between artificial and natural ECM, making the CHT/ALG/ACE+ELR more conducive to cell adhesion and growth.

4. Conclusions

CHT/ALG/ACE tubular architectures were successfully produced using freeze-drying methodology. The presented results indicate that a uniform and stable tubular structure free of defects (such as cracks and holes) can be achieved, demonstrating the effectiveness of the approach used. The proposed polymeric blended material and fabrication technique enables precise control over the graft's diameters by modifying the mold used. The designed structures support the hypothesis that blending different polymers in a molding solution allows for tailoring system behavior, properties, and degradation profiles.

The successful impregnation of ELRs resulted in a notable enhancement of the mechanical performance of the architectures. Furthermore, the bioactive potential of the system components, including polymers and peptides, facilitated the development of a multifunctional system, through their controlled release into the surrounding environment. A comparison of structures derived from various formulations revealed a reduction in porosity across the walls and interior of the tubes following the impregnation with proangiogenic ELRs. The ELRs, deposited on the surface and within the pores, acted as a functional coating without compromising the device's essencial role in nutrient and oxygen diffusion. The sustained release of the bioactive compounds, including ACE and ELRs, was ensured over time, which enhanced endothelial cells viability over time, further validating the system's potential.

This proof of concept confirms the feasibility of the proposed system for tissue engineering applications, particularly as a blood vessel substitute, pending further characterization. Future work will focus on verifying the clinical applicability of this system as a vascular graft. A systematic assessment of the construct's diameter range (from 3 mm to 10 mm) will determine its suitability for small- and medium-diameter applications. Evaluating the flow dynamics of the graft under simulated physiological conditions will be crucial for optimizing hemodynamic performance and minimizing thrombosis risk. Additionally, quantitative assessments of suture pull-out resistance, and durability through accelerated aging tests will offer deeper insights into the construct's long-term mechanical integrity and structural resilience. Complementary in vivo studies in animal models will ensure the graft's safety and efficacy for vascular reconstruction. These future studies will contribute with critical data to support the scalability and viability of this material as a durable vascular graft option.

CRediT authorship contribution statement

L.C. Rodrigues: Writing – review & editing, Writing – original draft, Visualization, Methodology, Investigation, Data curation, Conceptualization. **J.M. Gomes:** Methodology, Formal analysis, Data curation. **D. Soares da Costa:** Methodology, Formal analysis, Data curation, Writing – original draft. **E.M. Fernandes:** Methodology, Formal analysis, Data curation, Writing – original draft. **R.R. Costa:** Conceptualization, Methodology, Formal analysis, Data curation, Writing – original draft. **J. C. Rodriguez-Cabello:** Writing – review & editing, Funding acquisition. **S.S. Silva:** Conceptualization, Methodology, Writing – review & editing, Supervision. **R.L. Reis:** Supervision, Project administration, Funding acquisition.

Declaration of competing interest

The authors declare the following financial interests/personal relationships which may be considered as potential competing interests: Luisa Rodrigues reports financial support was provided by Portuguese FCT. Diana Costa reports financial support was provided by Portuguese FCT. Rui Costa reports financial support was provided by Portuguese FCT. Emanuel M. Fernandes reports financial support was provided by Portuguese FCT. Simone Silva reports financial support was provided by Portuguese FCT. Joana Gomes reports financial support was provided by Portuguese FCT. Rui L. Reis reports financial support was provided by European Commission. Rui L. Reis reports financial support was provided by Commission of the Coordination and Regional Development of the North. If there are other authors, they declare that they have no known competing financial interests or personal relationships that could have appeared to influence the work reported in this paper.

Acknowledgments

The authors especially acknowledge financial support from Portuguese FCT (PD/BD/135247/2017 (JMG), DL 57/2016/CP1377/CT0092 (D.S.C.) (DOI: 10.54499/DL57/2016/CP1377/CT0092) and DL 57/2016/CP1377/CT0054 (L.C.R) (DOI: 10.54499/DL57/2016/CP1377/CT0054); 2022.00764.CEECIND/CP1718/CT0020 (R.R.C.) (DOI: 10.54499/2022.00764.CEECIND/CP1718/CT0020); CEECINST/00018/2021/CP2806/CT0012 (S.S.S.) (DOI: 10.54499/CEECINST/00018/2021/CP2806/CT0012) and CEECINST/00018/2021/CP2806/CT0013 (E.M.F.) (DOI: 10.54499/CEECINST/00018/2021/CP2806/CT0013). This work is also financially supported by PhD programme in Advanced Therapies for Health (PATH) (PD/00169/2013), FCT R&D&I projects with references PTDC/BII-BIO/31570/2017, PTDC/CTM-CTM//29813/2017, PTDC/CTM-BIO/4706/2014-(POCI-01-0145-FEDER-016716), ELASTISLET (H2020-NMP-2014-two-stage-646075), and R&D&I Structured Projects with reference NORTE-01-0145-FEDER-000021. J.C.R.C was grateful for funding from the Spanish Government (PID2022-137484OB-I00).

The authors would also like to thank the contributions to this research from the project “TERM RES Hub – Scientific Infrastructure for Tissue Engineering and Regenerative Medicine”, reference PINFRA/22190/2016 (Norte-01-0145-FEDER-022190), funded by the Portuguese National Science Foundation (FCT) in cooperation with the Northern Portugal Regional Coordination and Development Commission (CCDR-N), for providing relevant lab facilities, state-of-the art equipment and highly qualified human resources.

Data availability

Data will be made available on request.

References

[1] A.J. Boys, S.L. Barron, D. Tilev, R.M. Owens, Building scaffolds for tubular tissue engineering, Front. Bioeng. Biotechnol. 8 (2020) 589960.
[2] L.C. Rodrigues, S.S. Silva, R.L. Reis, Acemannan-based films: an improved approach envisioning biomedical applications, Materials Research Express 6 (9) (2019) 095406.
[3] B. Yuan, Y. Jin, Y. Sun, D. Wang, J. Sun, Z. Wang, W. Zhang, X. Jiang, A strategy for depositing different types of cells in three dimensions to mimic tubular structures in tissues, Adv. Mater. 24 (7) (2012) 890–896.
[4] J.S. Boateng, K.H. Matthews, H.N.E. Stevens, G.M. Eccleston, Wound healing dressings and drug delivery systems: A review, J. Pharm. Sci. 97 (8) (2008) 2892–2923.
[5] T. Wang, X.-K. Zhu, X.-T. Xue, D.-Y. Wu, Hydrogel sheets of chitosan, honey and gelatin as burn wound dressings, Carbohydr. Polym. 88 (1) (2012) 75–83.
[6] C.Z. Bueno, A.M., Moraes, development of porous lamellar chitosan-alginate membranes: effect of different surfactants on biomaterial properties, J. Appl. Polym. Sci. 122 (2011) 624.
[7] P. Marie Arockianathan, S. Sekar, S. Sankar, B. Kumaran, T.P. Sastry, Evaluation of biocomposite films containing alginate and sago starch impregnated with silver nano particles, Carbohydr. Polym. 90 (1) (2012) 717–724.
[8] J.M. Silva, L.C. Rodrigues, S.S. Silva, R.L. Reis, A.R.C. Duarte, Engineered tubular structures based on chitosan for tissue engineering applications, J. Biomater. Appl. 32 (7) (2018) 841–852.
[9] J.M. Silva, C.A. Custodio, R.L. Reis, J.F. Mano, Multilayered hollow tubes as blood vessel substitutes, ACS Biomater Sci. Eng. 2 (12) (2016) 2304–2314.
[10] G.G. Flores-Rojas, B. Gómez-Lazaro, F. López-Saucedo, R. Vera-Graziano, E. Bucio, E. Mendizábal, Electrospun Scaffolds for tissue engineering: a review 3 (3) (2023) 524–553.
[11] A. Hasan, A. Memic, N. Annabi, M. Hossain, A. Paul, M.R. Dokmeci, F. Dehghani, A. Khademhosseini, Electrospun scaffolds for tissue engineering of vascular grafts, Acta Biomater. 10 (1) (2014) 11–25.
[12] P. Zorlutuna, P. Vadgama, V. Hasirci, Both sides nanopatterned tubular collagen scaffolds as tissue-engineered vascular grafts, J. Tissue Eng. Regen. Med. 4 (8) (2010) 628–637.
[13] C.E. Ghezzi, P.-A. Risse, B. Marelli, N. Muja, J.E. Barralet, J.G. Martin, S.N. Nazhat, An airway smooth muscle cell niche under physiological pulsatile flow culture using a tubular dense collagen construct, Biomaterials 34 (8) (2013) 1954–1966.
[14] C.E. Ghezzi, B. Marelli, N. Muja, S.N. Nazhat, Immediate production of a tubular dense collagen construct with bioinspired mechanical properties, Acta Biomater. 8 (5) (2012) 1813–1825.
[15] T.-J. Park, Y.J. Jung, S.-W. Choi, H. Park, H. Kim, E. Kim, S.H. Lee, J.H. Kim, Native chitosan/cellulose composite fibers from an ionic liquid via electrospinning, Macromol. Res. 19 (3) (2011) 213–215.
[16] W. He, Z. Ma, W.E. Teo, Y.X. Dong, P.A. Robless, T.C. Lim, S. Ramakrishna, Tubular nanofiber scaffolds for tissue engineered small-diameter vascular grafts, J. Biomed. Mater. Res. A 90 (1) (2009) 205–216.
[17] T. Xu, W. Zhao, J.-M. Zhu, M.Z. Albanna, J.J. Yoo, A. Atala, Complex heterogeneous tissue constructs containing multiple cell types prepared by inkjet printing technology, Biomaterials 34 (1) (2013) 130–139.
[18] K.-W. Lee, D.B. Stolz, Y. Wang, Substantial expression of mature elastin in arterial constructs, Proc. Natl. Acad. Sci. 108 (7) (2011) 2705–2710.
[19] L.A. Micol, M. Ananta, E.-M. Engelhardt, V.C. Mudera, R.A. Brown, J.A. Hubbell, P. Frey, High-density collagen gel tubes as a matrix for primary human bladder smooth muscle cells, Biomaterials 32 (6) (2011) 1543–1548.
[20] H. Yoshida, M. Matsusaki, M. Akashi, Multilayered blood capillary analogs in biodegradable hydrogels for in vitro drug permeability assays, Adv. Funct. Mater. 23 (14) (2013) 1736–1742.
[21] P.M. Crapo, Y. Wang, Physiologic compliance in engineered small-diameter arterial constructs based on an elastomeric substrate, Biomaterials 31 (7) (2010) 1626–1635.
[22] H. Ma, J. Hu, P.X. Ma, Polymer scaffolds for small-diameter vascular tissue engineering, Adv. Funct. Mater. 20 (17) (2010) 2833–2841.
[23] J.M. Silva, A.R.C. Duarte, C.A. Custódio, P. Sher, A.I. Neto, A. Pinho, J. Fonseca, R. L. Reis, J.F. Mano, Nanostructured hollow tubes based on chitosan and alginate multilayers, Adv. Healthc. Mater. 3 (3) (2014) 433–440.
[24] A.A. Barros, A. Rita, C. Duarte, R.A. Pires, B. Sampaio-Marques, P. Ludovico, E. Lima, J.F. Mano, R.L. Reis, Bioresorbable ureteral stents from natural origin polymers, Journal of Biomedical Materials Research Part B 103 (3) (2015) 608–617.
[25] Y. Song, M. Kamphuis, Z. Zhang, L.T. Sterk, I. Vermes, A. Poot, J. Feijen, D. Grijpma, Flexible and elastic porous poly (trimethylene carbonate) structures for use in vascular tissue engineering, Acta Biomater. 6 (4) (2010) 1269–1277.
[26] D.B. Camasão, D. Mantovani, The mechanical characterization of blood vessels and their substitutes in the continuous quest for physiological-relevant performances. A critical review, Materials Today Bio (2021) 100106.
[27] J.M. Gomes, C.F. Marques, L.C. Rodrigues, T.H. Silva, S.S. Silva, R.L. Reis, 3D bioactive ionic liquid-based architectures: an anti-inflammatory approach for early-stage osteoarthritis, Acta Biomater. 173 (2024) 298–313.
[28] B.C. Isenberg, C. Williams, R.T. Tranquillo, Small-diameter artificial arteries engineered in vitro, Circ. Res. 98 (1) (2006) 25–35.
[29] X. Zhang, X. Wang, V. Keshav, X. Wang, J.T. Johanas, G.G. Leisk, D.L. Kaplan, Dynamic culture conditions to generate silk-based tissue-engineered vascular grafts, Biomaterials 30 (19) (2009) 3213–3223.
[30] A.L. Larkin, R.M. Davis, P. Rajagopalan, Biocompatible, detachable, and free-standing polyelectrolyte multilayer films, Biomacromolecules 11 (10) (2010) 2788–2796.
[31] H. Kerdjoudj, C. Boura, V. Moby, K. Montagne, P. Schaaf, J.C. Voegel, J.F. Stoltz, P. Menu, Re-endothelialization of human umbilical arteries treated with polyelectrolyte multilayers: A tool for damaged vessel replacement, Adv. Funct. Mater. 17 (15) (2007) 2667–2673.
[32] J.M. Silva, R.L. Reis, J.F. Mano, Biomimetic extracellular environment based on natural origin polyelectrolyte multilayers, Small 12 (32) (2016) 4308–4342.
[33] S. Pashneh-Tala, S. MacNeil, F. Claeyssens, The tissue-engineered vascular graft-past, present, and future, Tissue Eng Part B Rev 22 (1) (2016) 68–100.
[34] Y. Zhang, Y. Liu, Z. Jiang, J. Wang, Z. Xu, K. Meng, H. Zhao, Poly(glyceryl sebacate)/silk fibroin small-diameter artificial blood vessels with good elasticity and compliance, Smart Materials in Medicine 2 (2021) 74–86.
[35] H.W. Toh, D.W.Y. Toong, J.C.K. Ng, V. Ow, S. Lu, L.P. Tan, P.E.H. Wong, S. Venkatraman, Y. Huang, H.Y. Ang, Polymer blends and polymer composites for cardiovascular implants, Eur. Polym. J. 146 (2021) 110249.
[36] L.C. Rodrigues, E.M. Fernandes, A.R. Ribeiro, A.P. Ribeiro, S.S. Silva, R.L. Reis, Physicochemical features assessment of acemannan-based ternary blended films for biomedical purposes, Carbohydr. Polym. 257 (2021) 117601.
[37] M.B. Dreifke, A.A. Jayasuriya, A.C. Jayasuriya, Current wound healing procedures and potential care, Materials Science & Engineering 48 (2015) 651–662.
[38] V. Patrulea, V. Ostafe, G. Borchard, O. Jordan, Chitosan as a starting material for wound healing applications, Eur. J. Pharm. Biopharm. 97 (2015) 417–426.
[39] M. Ali, S. Mir, O.-U.-R. Abid, A. Ajlouni, S. Ghafoor Alvi, S. Bibi, Applications of chitosan based bionanocomposites in drug-delivery and anticancer treatment-A review, Eur. Polym. J. 201 (2023) 112576.
[40] G.F. Caetano, M.A.C. Frade, T.A.M. Andrade, M.N. Leite, C.Z. Bueno, Â.M. Moraes, J.T. Ribeiro-Paes, Chitosan-alginate membranes accelerate wound healing, Journal of Biomedical Materials Research Part B 103 (5) (2015) 1013–1022.
[41] B. Kumar, N. Singh, P. Kumar, A review on sources, modification techniques, properties and potential applications of alginate-based modified polymers, Eur. Polym. J. 213 (2024) 113078.
[42] G.D. Sierra-Garcia, R. Castro-Rios, A. Gonzalez-Horta, J. Lara-Arias, A. Chavez-Montes, Acemannan, an extracted polysaccharide from Aloe vera: A literature review, Nat. Prod. Commun. 9 (8) (2014) 1217–1221.
[43] Y. Bai, Y. Niu, S. Qin, G. Ma, A new biomaterial derived from Aloe vera—Acemannan from basic studies to clinical application, Pharmaceutics 15 (7) (2023) 1913.
[44] L. Quintanilla-Sierra, C. García-Arévalo, J.C. Rodriguez-Cabello, Self-assembly in elastin-like recombinamers: a mechanism to mimic natural complexity, Materials Today Bio 2 (2019) 100007.
[45] S. Roberts, M. Dzuricky, A. Chilkoti, Elastin-like polypeptides as models of intrinsically disordered proteins, FEBS Lett. 589 (19PartA) (2015) 2477–2486.
[46] A. Tarakanova, W. Huang, A.S. Weiss, D.L. Kaplan, M.J. Buehler, Computational smart polymer design based on elastin protein mutability, Biomaterials 127 (2017) 49–60.
[47] L. De Rosa, R. Di Stasi, L.D. D'Andrea, Pro-angiogenic peptides in biomedicine, Arch. Biochem. Biophys. 660 (2018) 72–86.
[48] T. Flora, I.G. de Torre, M. Alonso, J.C. Rodríguez-Cabello, Tethering QK peptide to enhance angiogenesis in elastin-like recombinamer (ELR) hydrogels, J. Mater. Sci. Mater. Med. 30 (2) (2019) 30.
[49] R. Signini, S.P. Campana Filho, Características e propriedades de quitosanas purificadas nas formas neutra, acetato e cloridrato, Polímeros 11 (2001) 58–64.
[50] I. González de Torre, M. Santos, L. Quintanilla, A. Testera, M. Alonso, J. C. Rodríguez Cabello, Elastin-like recombinamer catalyst-free click gels: characterization of poroelastic and intrinsic viscoelastic properties, Acta Biomater. 10 (6) (2014) 2495–2505.
[51] T. Flora, I. González de Torre, M. Alonso, J.C. Rodríguez-Cabello, Use of proteolytic sequences with different cleavage kinetics as a way to generate hydrogels with preprogrammed cell-infiltration patterns imparted over their given 3D spatial structure, Biofabrication 11 (3) (2019) 035008.
[52] N.J. Agard, J.A. Prescher, C.R. Bertozzi, A strain-promoted [3 + 2] Azide−alkyne cycloaddition for covalent modification of biomolecules in living systems, J. Am. Chem. Soc. 126 (46) (2004) 15046–15047.
[53] F. González-Pérez, M. Alonso, I. González de Torre, M. Santos, J.C. Rodríguez-Cabello, Protease-sensitive, VEGF-mimetic peptide, and IKVAV laminin-derived peptide sequences within elastin-like recombinamer scaffolds provide spatiotemporally synchronized guidance of angiogenesis and neurogenesis 11 (22) (2022) 2201646.
[54] J.M. Gomes, S.S. Silva, L.C. Rodrigues, R.L. Reis, Alginate/acemannan-based beads loaded with a biocompatible ionic liquid as a bioactive delivery system, Int. J. Biol. Macromol. 242 (2023) 125026.
[55] S.M. Mousavi, S. Raveshiyan, Y. Amini, A. Zadhoush, A critical review with emphasis on the rheological behavior and properties of polymer solutions and their role in membrane formation, morphology, and performance, Adv. Colloid Interface Sci. 319 (2023) 102986.
[56] A.A. Salomé Machado, V.C.A. Martins, A.M.G. Plepis, Thermal and rheological behavior of collagen. Chitosan blends, J. Therm. Anal. Calorim. 67 (2) (2002) 491–498.

[57] M. Mucha, Rheological characteristics of semi-dilute chitosan solutions, Macromol. Chem. Phys. 198 (2) (1997) 471–484.
[58] A. Chenite, M. Buschmann, D. Wang, C. Chaput, N. Kandani, Rheological characterisation of thermogelling chitosan/glycerol-phosphate solutions, Carbohydr. Polym. 46 (1) (2001) 39–47.
[59] A.Y. Escobedo-Lozano, A. Domard, C.A. Velázquez, F.M. Goycoolea, W. M. Argüelles-Monal, Physical properties and antibacterial activity of chitosan/acemannan mixed systems, Carbohydr. Polym. 115 (2015) 707–714.
[60] F. Seidi, M. Khodadadi Yazdi, M. Jouyandeh, M. Dominic, H. Naeim, M.N. Nezhad, B. Bagheri, S. Habibzadeh, P. Zarrintaj, M.R. Saeb, M. Mozafari, Chitosan-based blends for biomedical applications, Int. J. Biol. Macromol. 183 (2021) 1818–1850.
[61] K. Enoch, R. C.S., A.A. Somasundaram, Tuning the rheological properties of chitosan/alginate hydrogels for tissue engineering application, Colloids Surf. A Physicochem. Eng. Asp. 697 (2024) 134434.
[62] J. Brugnerotto, J. Lizardi, F.M. Goycoolea, W. Argüelles-Monal, J. Desbrières, M. Rinaudo, An infrared investigation in relation with chitin and chitosan characterization, Polymer 42 (8) (2001) 3569–3580.
[63] J. Han, Z. Zhou, R. Yin, D. Yang, J. Nie, Alginate–chitosan/hydroxyapatite polyelectrolyte complex porous scaffolds: preparation and characterization, Int. J. Biol. Macromol. 46 (2) (2010) 199–205.
[64] S.G. Caridade, C. Monge, F. Gilde, T. Boudou, J.F. Mano, C. Picart, Free-standing polyelectrolyte membranes made of chitosan and alginate, Biomacromolecules 14 (5) (2013) 1653–1660.
[65] M.L. Duarte, M.C. Ferreira, M.R. Marvão, J. Rocha, An optimised method to determine the degree of acetylation of chitin and chitosan by FTIR spectroscopy, Int. J. Biol. Macromol. 31 (1) (2002) 1–8.
[66] S.S. Silva, L.C. Rodrigues, R.L. Reis, An alternative approach to prepare alginate/acemannan 3D architectures, SN Applied Sciences 1 (7) (2019) 684–693.
[67] R. Pereira, A. Tojeira, D.C. Vaz, A. Mendes, P. Bártolo, Preparation and characterization of films based on alginate and Aloe Vera, Int. J. Polym. Anal. Charact. 16 (7) (2011) 449–464.
[68] S.W. Jordan, C.A. Haller, R.E. Sallach, R.P. Apkarian, S.R. Hanson, E.L. Chaikof, The effect of a recombinant elastin-mimetic coating of an ePTFE prosthesis on acute thrombogenicity in a baboon arteriovenous shunt, Biomaterials 28 (6) (2007) 1191–1197.
[69] A.M. Testera, A. Girotti, I.G. de Torre, L. Quintanilla, M. Santos, M. Alonso, J. C. Rodríguez-Cabello, Biocompatible elastin-like click gels: design, synthesis and characterization, J. Mater. Sci. Mater. Med. 26 (2015) 1–13.
[70] Z. Wang, L. Liu, S.M. Mithieux, A.S. Weiss, Fabricating organized elastin in vascular grafts, Trends Biotechnol. 39 (5) (2021) 505–518.
[71] Y.-Y. Song, D. Liang, D.-K. Liu, L. Lin, L. Zhang, W.-Q. Yang, The role of the ERK signaling pathway in promoting angiogenesis for treating ischemic diseases 11 (2023).
[72] Z. Li, H.R. Ramay, K.D. Hauch, D. Xiao, M. Zhang, Chitosan-alginate hybrid scaffolds for bone tissue engineering, Biomaterials 26 (18) (2005) 3919–3928.
[73] P. Yadav, G. Beniwal, K.K. Saxena, A review on pore and porosity in tissue engineering, Materials Today: Proceedings 44 (2021) 2623–2628.
[74] D.B. Camasão, M. González-Pérez, S. Palladino, M. Alonso, J.C. Rodríguez-Cabello, D. Mantovani, Elastin-like recombinamers in collagen-based tubular gels improve cell-mediated remodeling and viscoelastic properties, Biomater. Sci. 8 (12) (2020) 3536–3548.
[75] D. Juanes-Gusano, M. Santos, V. Reboto, M. Alonso, J.C. Rodríguez-Cabello, Self-assembling systems comprising intrinsically disordered protein polymers like elastin-like recombinamers, J. Pept. Sci. 28 (1) (2022) e3362.
[76] S. Acosta, L. Quintanilla-Sierra, L. Mbundi, V. Reboto, J.C. Rodríguez-Cabello, Elastin-like recombinamers: deconstructing and recapitulating the functionality of extracellular matrix proteins using recombinant protein polymers 30 (44) (2020) 1909050.
[77] S. Jettanacheawchankit, S. Sasithanasate, P. Sangvanich, W. Banlunara, P. Thunyakitpisal, Acemannan stimulates gingival fibroblast proliferation; expressions of keratinocyte growth Factor-1, vascular endothelial growth factor, and type I collagen; and wound healing, J. Pharmacol. Sci. 109 (4) (2009) 525–531.
[78] S. Shafaie, S. Andalib, H. Shafaei, A. Montaseri, M. Tavakolizadeh, Differential biological behavior of fibroblasts and endothelial cells under aloe vera gel culturing, International journal of molecular and cellular medicine 9 (3) (2020) 234–246.
[79] T. Sugiura, R. Agarwal, S. Tara, T. Yi, Y.-U. Lee, C.K. Breuer, A.S. Weiss, T. Shinoka, Tropoelastin inhibits intimal hyperplasia of mouse bioresorbable arterial vascular grafts, Acta Biomater. 52 (2017) 74–80.
[80] C.J. Reddel, D. Cultrone, J. Rnjak-Kovacina, A.S. Weiss, J.K. Burgess, Tropoelastin modulates TGF-β1-induced expression of VEGF and CTGF in airway smooth muscle cells, Matrix Biol. 32 (7) (2013) 407–413.
[81] A.A. Thant, V. Ruangpornvisuti, P. Sangvanich, W. Banlunara, B. Limcharoen, P. Thunyakitpisal, Characterization of a bioscaffold containing polysaccharide acemannan and native collagen for pulp tissue regeneration, Int. J. Biol. Macromol. 225 (2023) 286–297.